Journal of Clinical and Translational Hepatology **2022** vol. 10(6) | 1167–1175
DOI: 10.14218/JCTH.2021.00499

Original Article

Preclinical Long-term Magnetic Resonance Imaging Study of Silymarin Liver-protective Effects

Yeon Ji Chae[1], Hwon Heo[1], Chul-Woong Woo[2], Sang-Tae Kim[2], Jae-Im Kwon[2], Monica Young Choi[1], Yu Sub Sung[3], Kyung Won Kim[4], Jeong Kon Kim[4], Yoonseok Choi[5*] and Dong-Cheol Woo[1,2*]

[1]Department of Convergence Medicine, Asan Medical Center, University of Ulsan College of Medicine, Seoul, Republic of Korea; [2]Convergence Medicine Research Center, Asan Institute for Life Sciences, Asan Medical Center, Seoul, Republic of Korea; [3]Clinical Research Center, Asan Medical Center, Seoul, Republic of Korea; [4]Department of Radiology, Asan Medical Center, University of Ulsan College of Medicine, Seoul, Republic of Korea; [5]Medical Research Institute, Gangneung Asan Hospital, Gangneung-si, Gangwon-do, Republic of Korea

Received: 4 November 2021 | **Revised:** 9 February 2022 | **Accepted:** 17 March 2022 | **Published:** 13 April 2022

Abstract

Background and Aims: Efficacy evaluations with preclinical magnetic resonance imaging (MRI) are uncommon, but MRI in the preclinical phase of drug development provides information that is useful for longitudinal monitoring. The study aim was to monitor the protective effectiveness of silymarin with multiparameter MRI and biomarkers in a thioacetamide (TAA)-induced model of liver injury in rats. Correlation analysis was conducted to assess compare the monitoring of liver function by MRI and biomarkers. ***Methods:*** TAA was injected three times a week for 8 weeks to generate a disease model (TAA group). In the TAA and silymarin-treated (TAA-SY) groups, silymarin was administered three times weekly from week 4. MR images were acquired at 0, 2, 4, 6, and 8 weeks in the control, TAA, and TAA-SY groups. ***Results:*** The area under the curve to maximum time (AUC_{tmax}) and T_2* values of the TAA group decreased over the study period, but the serological markers of liver abnormality increased significantly more than those in the control group. In the TAA-SY group, MRI and serological biomarkers indicated attenuation of liver function as in the TAA group. However, pattern changes were observed from week 6 to comparable levels in the control group with silymarin treatment. Negative correlations between either AUC_{tmax} or T_2* values and the serological biomarkers were observed. ***Conclusions:*** Silymarin had hepatoprotective effects on TAA-induced liver injury and demonstrated the usefulness of multiparametric MRI to evaluate efficacy in preclinical studies of liver drug development.

Citation of this article: Chae YJ, Heo H, Woo CW, Kim ST, Kwon JI, Choi MY, *et al*. Preclinical Long-term Magnetic Resonance Imaging Study of Silymarin Liver-protective Effects. J Clin Transl Hepatol 2022;10(6):1167–1175. doi: 10.14218/JCTH.2021.00499.

Introduction

Chronic liver diseases and their common consequent pathological characteristics, liver fibrosis and cirrhosis, are global health burdens.[1–3] Although numerous studies have yielded promising results regarding the prevention of disease progression by directly targeting viral infections or inhibiting hepatitis,[4–10] safe and effective drugs are still needed, as CLD morbidity is growing with the increasing prevalence of nonalcoholic steatohepatitis (NASH) and nonalcoholic fatty liver disease.[2,3,11,12]

Magnetic resonance imaging (MRI) is used to diagnose liver diseases because of its superior contrast resolution.[13,14] MRI provides morphological information and physiologic information to assess liver function,[15–18] and various MRI techniques have been used to evaluate novel liver drugs in development from the preclinical to the clinical phases.[19–21] Gadolinium ethoxybenzyl diethylenetriaminepentaacetic acid (Gd-EOB-DTPA)-enhanced T_1-weighted MRI, proton density fat fraction (PDFF) MRI, and T_2*-weighted MRI have all been used to measure liver functionality and pathologies.[22–27] Although all techniques are well established and have been used for liver imaging and functional assessment, preclinical liver and liver drug studies with MRI are still lacking compared with clinical liver MRI studies. However, as the importance of reliability between preclinical research and clinical outcomes increases, more preclinical MRI and translational research utilizing various imaging modalities may help the development of novel therapies for liver disease.[28–33]

Silymarin is a flavonolignan isolated from milk thistle seeds (*Silybum marianum*) that has been used to treat various liver diseases in preclinical and clinical studies owing to its anti-oxidative, anti-inflammatory, and antifibrotic ef-

Keywords: Liver fibrosis; Magnetic resonance imaging; Silymarin; T1-weighted dynamic contrast-enhanced; T_2*.

Abbreviations: ALB, albumin; ALT, alanine aminotransferase; AST, aspartate aminotransferase; AUC_{tmax}, area under the curve to maximum time; DCE, dynamic contrast-enhanced; GAPDH, glyceraldehyde 3-phosphate dehydrogenase; Gd-EOB-DTPA, gadolinium ethoxybenzyl diethylenetriaminepentaacetic acid; MRI, magnetic resonance imaging; TAA, thioacetamide; T_{max}, time to peak.

***Correspondence to:** Dong Cheol Woo, Convergence Medicine Research Center, Asan Institute for Life Sciences, Asan Medical Center 88, Olympic-ro 43-gil, Songpa-gu, Seoul 05505, Korea. ORCID: https://orcid.org/0000-0001-8202-015X. Tel: +82-2-3010-4155, Fax: +82-10-5559-7102, E-mail: dcwoo@amc.seoul.kr; Yoonseok Choi, Medical Research Institute, Gangneung Asan Hospital, University of Ulsan College of Medicine 38, Bangdong-gil, Sacheon-myeon, Gangneung-si, Gangwon-do 25440, Korea. ORCID: https://orcid.org/0000-0002-8478-2999. Tel: +82-33-610-4799, Fax: +82-33-610-3089, E-mail: yschoi21rad@gnah.co.kr

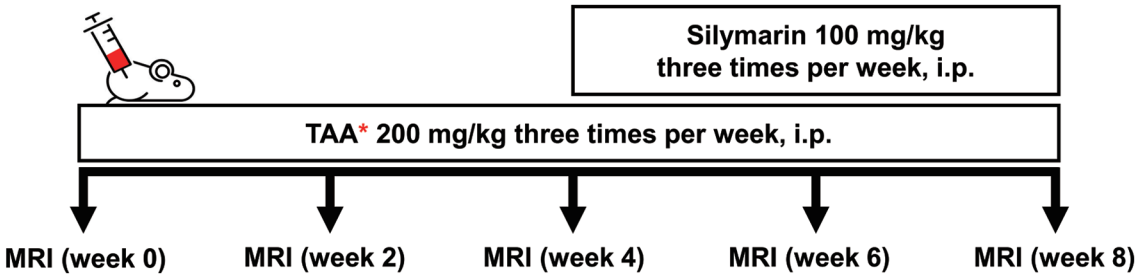

Fig. 1. Scheme of the TAA-induced hepatic fibrosis animal model. i.p., intraperitoneal injection; MRI, magnetic resonance imaging; TAA, thioacetamide.

fects.[34–36] Silymarin protects cell membranes from damage caused by reactive oxygen species and inhibits free radical formation. It also exerts anti-inflammatory activity by preventing cellular NF-kB activation, thereby inhibiting the activation of hepatic stellate cells and recruitment of other pro-inflammatory immune cells. Moreover, silymarin has an antifibrotic effect through the inhibition of myofibroblast activities. It prevents the transformation of hepatic stellate cells to a myofibroblast-like phenotype and blocks the generation of the extracellular matrix that induces hepatic fibrosis. However, no studies have evaluated the effects of silymarin on liver function with 8 weeks of follow-up MRIs. Moreover, correlative relation analysis with longitudinal MRI data and other traditional serological and histological biomarkers of liver function have not been done in previous studies. Herein, we investigated the protective effects of silymarin in a thioacetamide (TAA)-induced animal model longitudinally with MRI. In addition, we analyzed the correlations between biomarkers and multiparametric MRI data and assessed the interpretability of biomarkers and MRI values reflecting disease severity.

Methods

TAA-induced fibrosis animal model and silymarin administration

We purchased 6-week-old male Sprague-Dawley (SD) rats from the Orient Animal Laboratory (Seoul, South Korea). The SD-rats were randomly divided into three groups, controls (n=9), TAA-injected (n=13, TAA group), and TAA-injected, silymarin-treated (n=11, TAA-SY group). To induce hepatic fibrosis, 200 mg/kg thioacetamide (TAA, 163678, Sigma-Aldrich, St. Louis, MO, USA) was intraperitoneally injected three times a week for 8 weeks. After 4 weeks, 100 mg/kg of silymarin (SY, S0292, Sigma-Aldrich, St. Louis, MO, USA) was intraperitoneally administered three times a week for four weeks (Fig. 1). The silymarin administration protocol was determined based on previous studies that showed the liver-protective effects of silymarin.[37,38] All animal experimental procedures were approved by the Committee on the Ethics of Animal Experiments at Asan Medical Center (IACUC No. 2018-12-115).

Biochemical analysis

Blood samples were collected from the tail vein every 2 weeks. Whole blood samples were collected in BD serum separation tubes (Becton Dickinson, Franklin Lakes, NJ, USA) and blood was allowed to clot for 30 m and centrifuged at 3,000 rpm for 10 m. We measured serum levels of aspartate aminotransferase (AST), alanine aminotransferase (ALT), and albumin (ALB) with a Hitachi 7180 Autoanalyzer (Hitachi Ltd., Tokyo, Japan).

Histological analysis

Liver tissue samples were fixed in 4% paraformaldehyde, paraffin-embedded, sectioned at 4 μm and stained with hematoxylin and eosin (H&E) or Masson's trichrome (MT) following standard procedures. Stained slides were scanned with a Vectra imaging system (PerkinElmer, Waltham, MA, USA). Lobular inflammation (0–3), ballooning (0–2), and fibrosis (0–4) were graded. Lobular inflammation was scored as no foci (score 0), <2 foci/200× (score 1), 2–4 foci/200× (score 2), and >4 foci/200× (score 3). Hepatocyte ballooning was scored as none (score 0), few ballooned cells (score 1), or many ballooned cells (score 2). Fibrosis stage was graded as described by Brunt *et al*.[39] as none (stage 0), portal fibrosis (stage 1), portal fibrosis with few septa (stage 2), septal or bridging fibrosis (stage 3), or cirrhosis (stage 4). Prussian blue staining was carried out with a staining kit (ab150674, Abcam, Cambridge, MA, USA) following the manufacturer's protocol. Iron quantification was performed by measuring Prussian blue-positive regions in photographs using ImageJ software (National Institutes of Health, Bethesda, MD, USA).

Western blotting

Liver tissue was homogenized in RIPA lysis buffer (Thermo Fisher Scientific, Rockford, IL, USA) supplemented with protease and phosphatase inhibitors. Western blots reacted with primary antibodies against ferritin (3998S, Cell Signaling Technology, Beverly, MA, USA), hepcidin (M01347, Boster Biological Technology, Pleasanton, CA, USA) and GAPDH (ab8245, Abcam, USA), followed by HRP-conjugated secondary antibodies. The results were read with an image analyzer (Image lab 3.0, Bio-Rad, Hercules, CA, USA) and blots were quantified with ImageJ.

MRI

MRI was performed every 2 weeks using a 9.4-T magnet (Agilent, Inc., Santa Clara, CA, USA) with a 64 mm transmit/receive volume coil. Animals were anesthetized with a 1.5–2% isoflurane/air mixture during the imaging session, body temperature was maintained at 37.5±0.5°C with an air heater system, and the respiratory rate was monitored to adjust the anesthetic concentration. T1-weighted dynamic contrast-enhanced (DCE)-MRI were obtained after the administration of 25 μmol/kg Gd-EOB-DTPA (Primovist, Bayer Healthcare, Leverkusen, Germany) by intravenous injection after 120 s. The MRI parameters were: (1) T1-weighted

Table 1. Repeated measures analysis of variance of the AUC_{tmax} in the three groups

	AUC_{tmax} (%)								
	Control (G1)		TAA (G2)		TAA+SY (G3)		G1 vs. G2	G1 vs. G3	G2 vs. G3
	Mean	SD	Mean	SD	Mean	SD		*p*	
Week 0	1.00	0.14	1.00	0.25	1.00	0.21	n.s	n.s	n.s
Week 2	0.97	0.18	0.76	0.21	0.72	0.17	n.s	n.s	n.s
Week 4	1.09	0.26	0.70	0.14	0.66	0.12	<0.001	<0.001	n.s
Week 6	0.94	0.12	0.67	0.24	0.72	0.10	0.049	n.s	n.s
Week 8	1.08	0.20	0.56	0.12	0.84	0.13	<0.001	0.005	p0.033
RM-ANOVA	F=1.055		F=5.781		F=3.977		*<0.05, **<0.01, ***<0.001		
	p=0.395		*p*=0.001***		*p*=0.013*				

RM-ANOVA with F-value (*F*) and *p*-value (p) (*p<0.05, **p<0.01, ***p<0.001). AUC_{tmax}, area under the curve to maximum time; n.s, not significant; RM-ANOVA, repeated measures analysis of variance; TAA, thioacetamide-injected; TAA-SY, TAA-injected and silymarin-treated.

DCE-MRIs with TR/TE=70/2.34 ms, flip angle=35°, averages=1, matrix size=96×96, field-of-view (FOV)=50×50 mm^2 (resolution: 0.52 mm), total scan time=44 min 48 s, and the number of images=400; and (2) T_2* maps with TR/TE=800/2.56 ms, echo=6, flip angle=30°, averages=4, matrix size 128×128, and FOV=50×50 mm^2 (resolution: 0.39 mm).

MRI analysis

The MRI data (AUC_{tmax} and T_2*) were analyzed with ImageJ. Two regions of interest (ROIs) were randomly placed in the liver and were measured, avoiding visible blood vessels. The relative enhancement rate (RER) was calculated using the equation RER(t)=[{SI(t) − SI(0)} / SI(0)] × 100 (%),[33] where SI(t) is the signal intensity of the liver at time t and SI(0) is the average of SI before Gd-EOB-DTPA injection. The area under the curve to maximum time (AUC_{t-max}) was calculated by the integration of areas from 0–6 m. The time to peak (T_{max}) was calculated using Analysis of Functional NeuroImages Software (http://afni.nimh.nih.gov/afni).

Statistical analysis

Statistical analysis was performed with IBM SPSS for Windows version 21.0 (IBM Corp., Armonk, NY, USA). To evaluate the changes in parameters over time, we performed a comparison using repeated measures analysis of variance. One-way analysis of variance, and independent *t*-tests were performed to compare mean values, and p<0.05 was considered statistically significant.

Results

Biochemical assessment of liver function-related biomarkers

Biochemical assays were performed to evaluate liver function and to analyze the correlation between serum markers and MRI data. In the control group, aspartate aminotransferase (AST), alanine aminotransferase (ALT), and albumin (ALB) levels remained the same from week 1 to week 8 of the study. In the TAA group, AST and ALT gradually increased, but the ALB level remained constant. In the TAA-SY group, AST and ALT increased until week 4, and their levels decreased with the initiation of silymarin (Supplementary Table 1). AST and ALT levels in the TAA group were significantly higher compared with the other groups during the last week of the study (Fig. 2A and Supplementary Table 1). After the animals were euthanized, histological analysis showed inflammatory cell infiltration and fibrous septa in the TAA-treated groups (TAA and TAA-SY). The NAS scores for lobular inflammation (0.00±0.00 vs. 2.29±0.83 vs. 1.55±0.69) and Brunt scores for fibrosis degree (0.22±0.44 vs. 3.29±0.73 vs. 2.36±1.03) in the three study groups were significantly higher in the TAA group than in the other two groups (Fig. 2B and Supplementary Table 2).

Gd-EOB-DTPA-enhanced T_1-weighted MRI for liver function assessment

Parallel to the serological marker assays and histological analysis, we performed T_1-weighted MRI of ROIs in the liver parenchyma (Fig. 3A). Comparative analysis found that the TAA group had a lower RER than the control group from week 2 onward and that the TAA-SY group showed recovery from week 6 (Fig. 3B). The AUC_{tmax} values were maintained at similar levels for 8 weeks in the control group (F=1.055, p=0.395). The TAA group showed gradual decreases following TAA injection (F=5.781, ***p=0.001). In the TAA-SY group, AUC_{tmax} showed recovering patterns from the week 6, which was 2 weeks after silymarin injection (F=3.977, *p=0.013). In the group comparison, the AUC_{tmax} levels in the TAA group significantly decreased from week 4 onward compared with the control group. In the TAA-SY group, there was a significant decrease in the AUC_{tmax} compared with the control group at week 4. As the levels of AUC_{tmax} recovered after week. 6, we observed significant differences between the TAA and TAA-SY groups. However, the AUC_{tmax} did not recover to the levels of the control group at week 8 (Fig. 3C and Table 1). A delay of the peak (T_{max}) was not observed (Fig. 3D and Supplementary Table 3) in the experiment. We observed negative correlations between AUC_{tmax} and each AST (R=−0.4605, ***p<0.0001) and ALT (R=−0.3608, ***p<0.0001; Fig. 3E).

T_2 mapping MRI for liver function assessment*

We included T_2* mapping MR images in a multiparametric analysis (Fig. 4A). Similar patterns were observed in

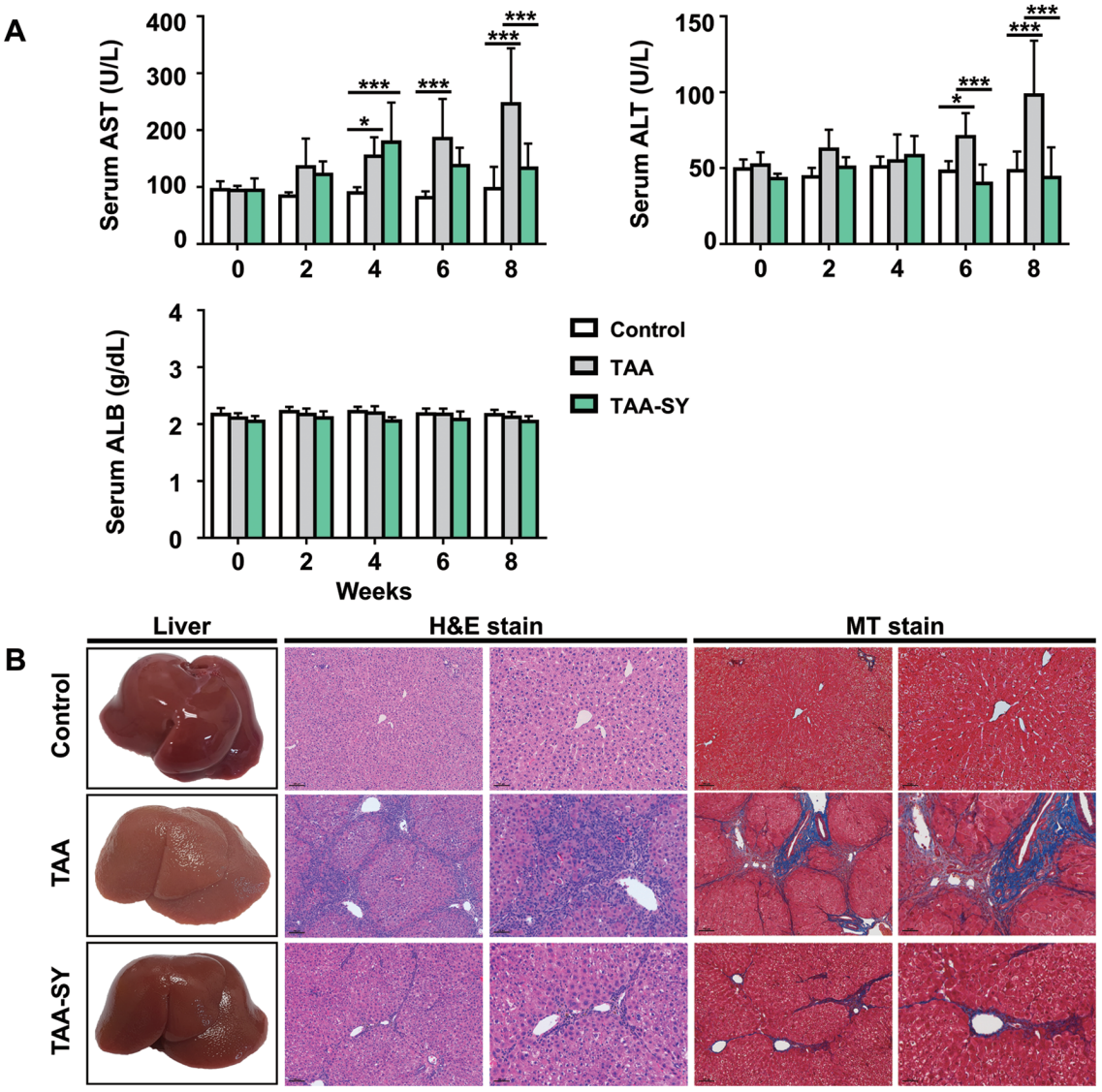

Fig. 2. Comparison of the expression of serological markers and histological analysis in the experimental groups. (A) Compared with the control group, the TAA group showed increased serum levels of AST and ALT; however, the TAA-SY group recovered at weeks 6 and 8, and serum ALB levels were not different (*p<0.05, **p<0.01, ***p<0.001). (B) Representative hematoxylin and eosin and Masson's trichrome staining showing inflammation and fibrosis areas (nodules). ALB, albumin; ALT, alanine aminotransferase; AST, aspartate aminotransferase; TAA, thioacetamide-injected; TAA-SY, TAA-injected and silymarin-treated.

the T_2* values compared with T_1-weighted images. Fairly constant levels of T_2* values were observed in the control group for 8 weeks (F=1.370, p=0.264) and gradual decreases in the T_2* values were observed in the TAA group (F=60.214, ***p<0.001). The values of the TAA-SY group showed a tendency of recovery from week 6 (F=12.325, ***p<0.001). In the group comparison, the T_2* values were significantly lower in the TAA group compared with the control group from week 2. Also, the TAA-SY group showed a gradual decrease of T_2* values compared with the control group. No significant differences were observed in the T_2* values between the TAA group and TAA-SY group. However, the T_2* values of the TAA-SY group increased after week 6, eventually becoming significantly higher at week 8 (Fig. 4B and Table 2). Significant negative correlations between the T_2* and AST (R=−0.6200, ***p<0.0001) and ALT (R=−0.5617, ***p<0.0001) were observed (Fig. 4C).

*Iron accumulation in the liver and correlation with T_2**

We further analyzed iron accumulation in the liver and its correlation with T_2* shortening. We observed iron overload near the portal triad of fibrosis in the liver in both TAA-treated groups (TAA and TAA-SY) with Prussian blue staining (Fig. 5A). We also observed significant iron accumulation in both TAA-treated groups compared with the control group (0.39±0.24 control vs. 6.23±3.30 TAA, ***p<0.001; 0.39±0.24 control vs. 3.23±1.73 TAA-SY; *p=0.03). However, iron accumulation was significantly lower in the TAA-SY than in the TAA group (6.23±3.30 TAA vs. 3.23±1.73 TAA-SY, *p=0.011; Fig. 5B). We measured ferritin and hepcidin levels to assess iron storage and homeostasis. The highest expression level of ferritin, the iron storage protein, was observed in the TAA group compared with the control (*p=0.047) and TAA-SY (*p=0.038) groups. The expression of hepcidin, the

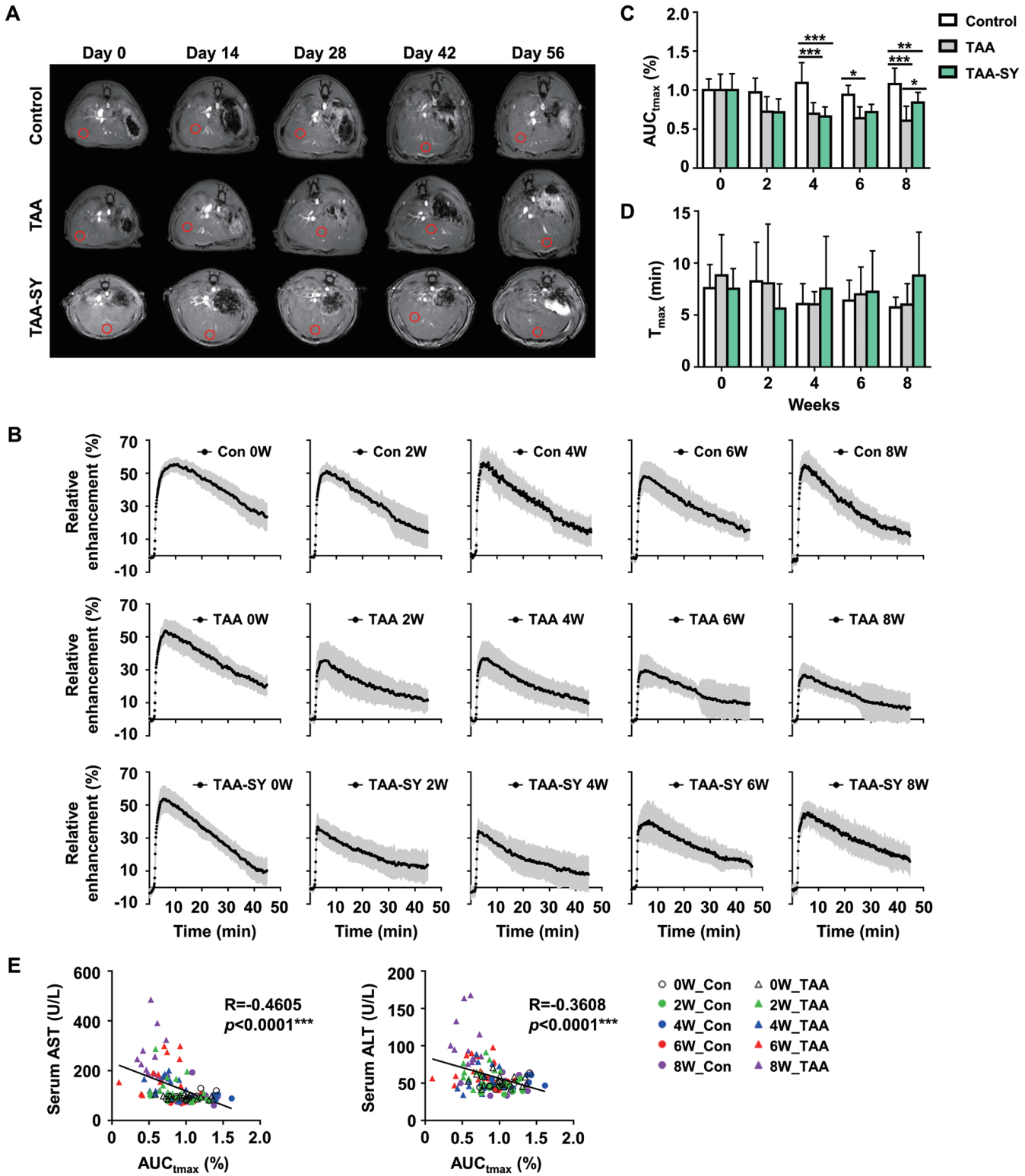

Fig. 3. GD-EOB-DTPA-enhanced T1-weighted DCE-MRI following TAA and silymarin injection. (A) Axial MRI of the liver with a region of intensity (ROI; red box) obtained for longitudinal study of the control, TAA, and TAA-SY groups on days 0, 14, 28, 42, and 56. (B) Relative enhancement rate (RER) was analyzed in T_1-weighted DCE images. (C) AUC_{tmax} was decreased in the TAA group and increased in the TAA-SY group at 8 weeks (*p<0.05, **p<0.01, ***p<0.001). (D) T_{max} did not differ among the three groups. (E) Pearson correlation coefficients (r) and p-values for the control and TAA groups during TAA induction. The AUC_{tmax} correlated with the expression of several hepatic enzymes (*p<0.05, **p<0.01, ***p<0.001). ALT, alanine aminotransferase; AST, aspartate aminotransferase; AUC_{tmax}, area under the curve to maximum time; Con, control; TAA, thioacetamide-injected; TAA-SY, TAA-injected and silymarin-treated; T_{max}, time to peak.

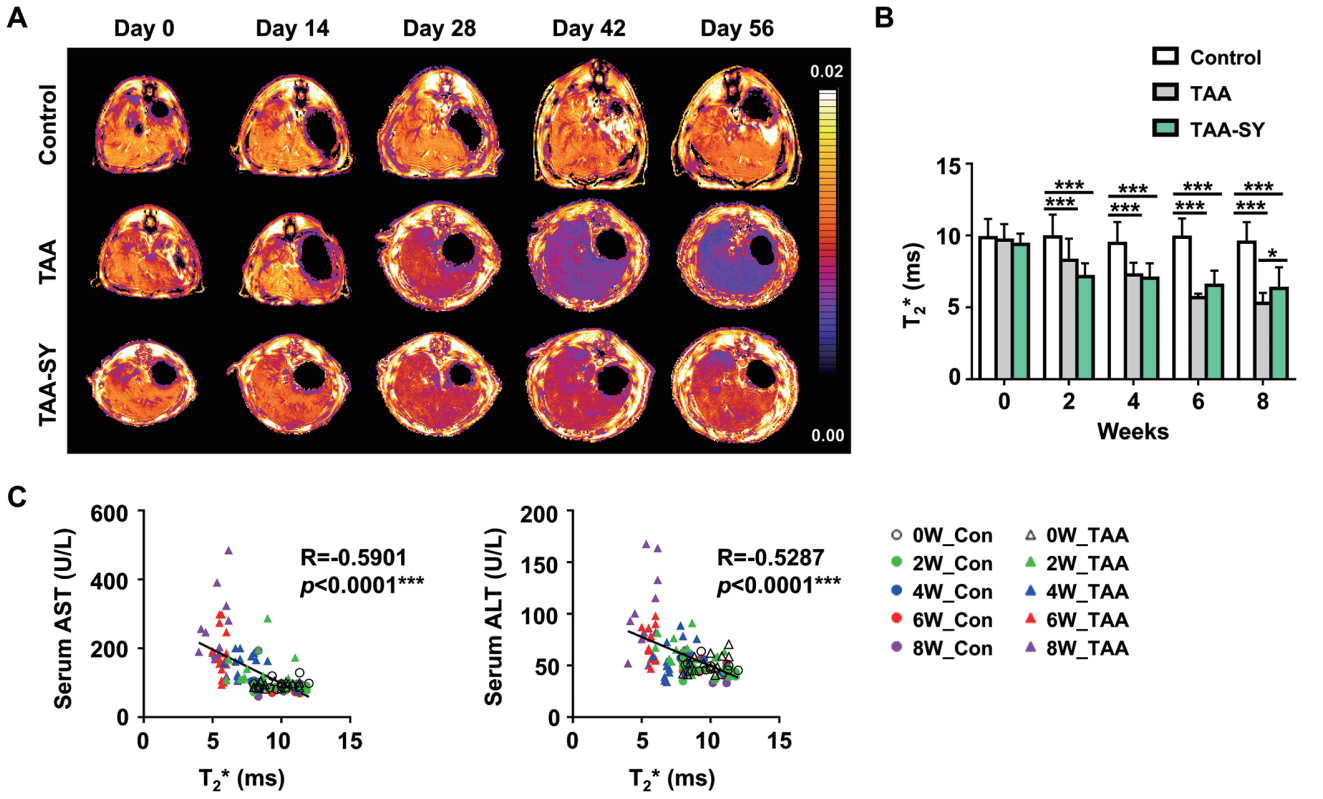

Fig. 4. T_2* value map following TAA and silymarin injection. (A) An axial MRI was obtained for all groups. (B) T_2* values were reduced in the TAA group compared with the control group, and increased in the TAA-SY group at 6 and 8 weeks compared with the TAA group (*p<0.05, **p<0.01, ***p<0.001). (C) T_2* values correlated with the expression of several hepatic enzymes (*p<0.05, **p<0.01, ***p<0.001). ALT, alanine aminotransferase; AST, aspartate aminotransferase; Con, control; TAA, thioacetamide-injected; TAA-SY, TAA-injected and silymarin-treated.

negative regulator for iron release, was not significantly altered, but the lowest expression was observed in the TAA group compared with the other two groups (Fig. 5C, D). The T_2* values and hepatic iron accumulation (% area) in the control, TAA, and TAA-SY groups at week 8 negatively correlated (R=−0.7010, ***p<0.0001; Fig. 5E).

Discussion

We monitored the liver-protective effects of silymarin with longitudinal MRI follow-up and monitoring of liver function biomarkers. We observed meaningful correlations between MRI-based values and the levels of several biomarkers. Carbon tetrachloride (CCl_4) is frequently used to induce liver failure,[40–42] but liver function occasionally occurs when CCl_4 administration is stopped.[42] Conversely, TAA damage persists for more than 2 months after withdrawal, and induces pathological characteristics similar to human chronic liver dysfunction. TAA-induced liver injury models are thus more suitable than CCl_4 for longitudinal studies. We did not show the results of more than one concentration of silymarin as

Table 2. Repeated measures analysis of variance of T_2* values in the three groups

	T_2* (ms)								
	Control (G1)		TAA (G2)		TAA+SY (G3)		G1 vs. G2	G1 vs. G3	G2 vs. G3
	Mean	SD	Mean	SD	Mean	SD	*p*		
Week 0	9.84	1.32	9.68	1.12	9.38	0.75	n.s	n.s	n.s
Week 2	9.91	1.55	8.28	1.50	7.15	0.92	0.027	<0.001	n.s
Week 4	9.45	1.49	7.26	0.84	7.03	1.04	0.001	<0.001	n.s
Week 6	9.88	1.30	5.68	0.28	6.53	1.02	<0.001	<0.001	n.s
Week 8	9.53	1.40	5.05	0.72	6.74	1.48	<0.001	<0.001	0.035
RM-ANOVA	F=1.370		F=60.214		F=12.325		*<0.05, **<0.01, ***<0.001		
	p=0.264		*p*<0.001***		*p*<0.001***				

RM-ANOVA with F-value (F) and p-value (p) (*p<0.05, **p<0.01, ***p<0.001). n.s, not significant; RM-ANOVA, repeated measures analysis of variance; TAA, thioacetamide-injected; TAA-SY, TAA-injected and silymarin-treated.

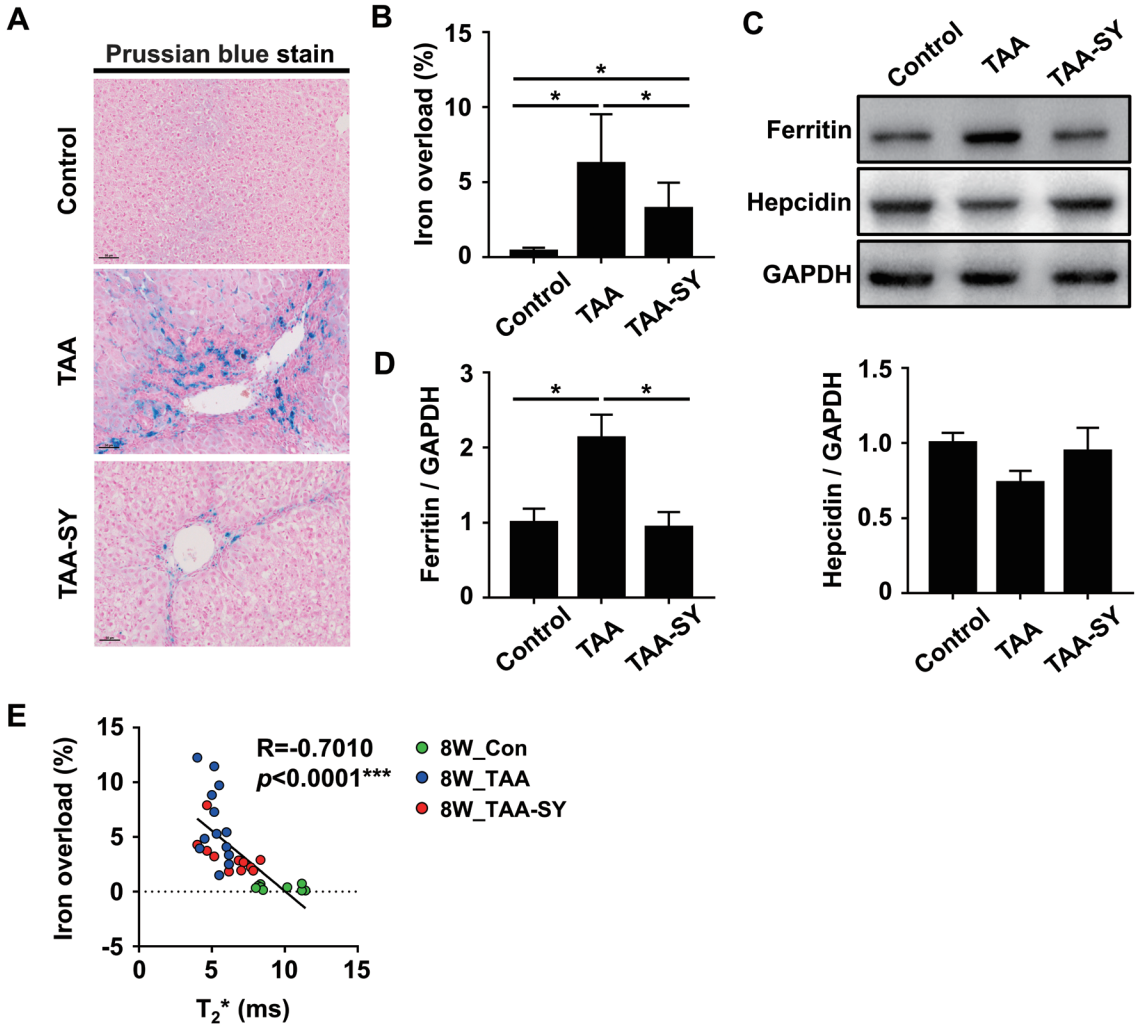

Fig. 5. Changes in iron overload in the TAA-SY group. (A) Prussian blue staining evaluated iron accumulation. (B) Iron accumulation significantly decreased in the TAA-SY group compared with the TAA group. (C) Western blot assays of ferritin and hepcidin protein expression. (D) Ferritin in the TAA-SY group was decreased compared with the TAA group. Hepcidin in the TAA-SY group was slightly increased compared with the TAA group. (E) T_2* values and iron overload (%) were negatively correlated (*p<0.05, **p<0.01, ***p<0.001). Con, control; GAPDH, glyceraldehyde 3-phosphate dehydrogenase; TAA, thioacetamide-injected; TAA-SY, TAA-injected and silymarin-treated.

we designed our study to avoid the complexities associated with multi-dosages. We observed changes in serological biomarkers that reflected the liver-protective effects of silymarin at 100 mg/kg. We also observed reduced fibrosis and infiltration of inflammatory cells in H&E stained tissue. The results are consistent with previous studies of silymarin treatment in induced liver injury models.[34,38] The anti-oxidative, anti-inflammatory, and anti-fibrotic effects of silymarin were evident throughout the study period.

Gadoxetate-enhanced T1-weighted MRI images are used to assess liver function because of their implicative representations of the contrast agent-transporting abilities of hepatocytes. The maximum RER values in the TAA group were reduced after TAA injection. In the TAA-SY group, lowered the RERs; however, silymarin treatment led to a gradual RER recovery to levels similar to those of the control group. The AUC_{tmax} values showed patterns equivalent to those of the level change patterns of RERs. In the latter period of the experiment, the AUC_{tmax} of the TAA group was significantly lower compared to those of the other two groups. Although several studies refer to T1-weighted MRI as an extremely useful tool for liver function assessment,[28,43] we analyzed the correlation between the MRI data and serological markers to assess the relationship between MRI and liver function. AUC_{tmax}, AST, and ALT showed significant negative correlations, which confirmed an association between the lowered T1 values and elevated enzyme levels resulting from liver dysfunction. Cumulatively, the results indicate that the contrast agent uptake into the hepatocytes was hindered after TAA injection. The resulting liver dysfunction caused changes of the T1-weighted image data.

Several clinical and preclinical studies have reported that iron metabolism is disturbed in chronic hepatic diseases.[44–46] Iron accumulation becomes significant with the progression of fibrosis severity, and excessive iron accumulation induces fibrosis-promoting oxidative stress. This iron-dependent cell death loop causes ongoing cellular and tissue damage to the liver. The release of iron from the dead cells and accumulation in the interstitial space of the liver shortens the T_2* in the MRI. Consistent with the results of many studies that measure the iron overload with MRI,[47,48] we also observed gradual decreases in T_2* along the ex-

perimental period in the TAA group. A decrease of T_2* was also observed in the TAA-SY group; however, the degree of decrease became smaller, and significant differences were noted compared with the values of the TAA group at eight weeks. Negative correlations were observed between the T_2* values and the serological biomarkers and between AUC_{tmax} and the serological biomarkers. However, the T_2* values in the TAA-SY group did not recover to the levels of the control group at the week 8, although a significant difference existed between the TAA and TAA-SY groups. The Prussian blue staining results indicate that the amount of iron residing in the extracellular matrices explained the lowered T_2* values in the TAA-SY group compared with the control group. Moreover, the expression patterns of ferritin and hepcidin supported the iron accumulation status of the three groups, as higher ferritin expression levels imply that cells store more iron. Lower expression of hepcidin implies that the iron release inside the liver was redundant.

Considering the different patterns in AUC_{tmax} and T_2* values, silymarin treatment appears to have caused the time differences in the recovery of hepatocyte transporting abilities and in accumulated iron clearance in the interstitial space. To elucidate the precise reason for this phenomenon, further studies are needed.

In line with other studies, we found that silymarin had hepatoprotective effects[36,49,50] and that MRI was highly useful for assessing liver function and drug efficacy. Although preclinical studies of new liver disease drugs using MRI are limited, the applications of MRI will increase along with the increasing need for new drugs to combat chronic liver diseases. Further studies are necessary if new MRI techniques develop to assess liver function, and we expect that additional studies will broaden the scope of MRI use in the future.

Acknowledgments

We thank the core facilities of the Magnetic Resonance Core and the Comparative Pathology Core at the ConveRgence mEDIcine research center (CREDIT), Asan Medical Center for the use of their shared equipment, services and expertise.

Funding

This work was supported by grants from the Asan Institute of Life Sciences, Asan Medical Center, Republic of Korea (2020IL0026-1); the Basic Science Research Program through the National Research Foundation of Korea (NRF) funded by the Ministry of Science and ICT (2018R1A2B2007694); and the Ministry of Education (2020R1I1A1A01058302).

Conflict of interest

The authors have no conflict of interests related to this publication.

Author contributions

Study concept and design (DCW, YC), acquisition of data (YJC, JIK, MYC), analysis and interpretation of data (YJC, HH), manuscript drafting (YC, YJC), magnetic resonance imaging (WCW, STK), critical revision of the manuscript for important intellectual content (HH, YC), and administrative, technical, or material support and study supervision (YSS, KWK, DCW, YC). All authors contributed important intellectual content and approved the submission of this manuscript.

Data sharing statement

All data are available upon request.

References

[1] Asrani SK, Devarbhavi H, Eaton J, Kamath PS. Burden of liver diseases in the world. J Hepatol 2019;70(1):151–171. doi:10.1016/j.jhep.2018.09.014, PMID:30266282.
[2] Marcellin P, Kutala BK. Liver diseases: A major, neglected global public health problem requiring urgent actions and large-scale screening. Liver Int 2018;38(Suppl 1):2–6. doi:10.1111/liv.13682, PMID:29427496.
[3] Paik JM, Golabi P, Younossi Y, Mishra A, Younossi ZM. Changes in the Global Burden of Chronic Liver Diseases From 2012 to 2017: The Growing Impact of NAFLD. Hepatology 2020;72(5):1605–1616. doi:10.1002/hep.31173, PMID:32043613.
[4] Chatterjee R, Mitra A. An overview of effective therapies and recent advances in biomarkers for chronic liver diseases and associated liver cancer. Int Immunopharmacol 2015;24(2):335–345. doi:10.1016/j.intimp.2014.12.024, PMID:25560752.
[5] Lambrecht J, van Grunsven LA, Tacke F. Current and emerging pharmacotherapeutic interventions for the treatment of liver fibrosis. Expert Opin Pharmaco 2020;21(13):1637–1649. doi:10.1080/14656566.2020.1774553 , PMID:32543284.
[6] Damiris K, Tafesh ZH, Pyrsopoulos N. Efficacy and safety of anti-hepatic fibrosis drugs. World J Gastroenterol 2020;26(41):6304–6321. doi:10.3748/wjg.v26.i41.6304, PMID:33244194.
[7] Nguyen MH, Wong G, Gane E, Kao JH, Dusheiko G. Hepatitis B Virus: Advances in Prevention, Diagnosis, and Therapy. Clin Microbiol Rev 2020;33(2):e00046–19. doi:10.1128/CMR.00046-19, PMID:32102898.
[8] Dennis BB, Naji L, Jajarmi Y, Ahmed A, Kim D. New hope for hepatitis C virus: Summary of global epidemiologic changes and novel innovations over 20 years. World J Gastroenterol 2021;27(29):4818–4830. doi:10.3748/wjg.v27.i29.4818, PMID:34447228.
[9] Do A, Reau NS. Chronic Viral Hepatitis: Current Management and Future Directions. Hepatol Commun 2020;4(3):329–341. doi:10.1002/hep4.1480, PMID:32140652.
[10] Thiagarajan P, Aithal GP. Drug Development for Nonalcoholic Fatty Liver Disease: Landscape and Challenges. J Clin Exp Hepatol 2019;9(4):515–521. doi:10.1016/j.jceh.2019.03.002, PMID:31516268.
[11] Younossi Z, Anstee QM, Marietti M, Hardy T, Henry L, Eslam M, *et al*. Global burden of NAFLD and NASH: trends, predictions, risk factors and prevention. Nat Rev Gastroenterol Hepatol 2018;15(1):11–20. doi:10.1038/nrgastro.2017.109, PMID:28930295.
[12] Roeb E. Non-alcoholic fatty liver diseases: current challenges and future directions. Ann Transl Med 2021;9(8):726. doi:10.21037/atm-20-3760, PMID:33987424.
[13] Laing AD, Gibson RN. MRI of the liver. J Magn Reson Imaging 1998;8(2):337–345. doi:10.1002/jmri.1880080213, PMID:9562060.
[14] Vu LN, Morelli JN, Szklaruk J. Basic MRI for the liver oncologists and surgeons. J Hepatocell Carcinoma 2017;5:37–50. doi:10.2147/JHC.S154321, PMID:29692983.
[15] Taouli B, Ehman RL, Reeder SB. Advanced MRI methods for assessment of chronic liver disease. AJR Am J Roentgenol 2009;193(1):14–27. doi:10.2214/AJR.09.2601, PMID:19542391.
[16] Maniam S, Szklaruk J. Magnetic resonance imaging: Review of imaging techniques and overview of liver imaging. World J Radiol 2010;2(8):309–322. doi:10.4329/wjr.v2.i8.309, PMID:21160685.
[17] Petitclerc L, Gilbert G, Nguyen BN, Tang A. Liver Fibrosis Quantification by Magnetic Resonance Imaging. Top Magn Reson Imaging 2017;26(6):229–241. doi:10.1097/RMR.0000000000000149, PMID:28858038.
[18] Zhou IY, Catalano OA, Caravan P. Advances in functional and molecular MRI technologies in chronic liver diseases. J Hepatol 2020;73(5):1241–1254. doi:10.1016/j.jhep.2020.06.020, PMID:32585160.
[19] Galbraith SM. MR in oncology drug development. NMR Biomed 2006;19(6):681–689. doi:10.1002/nbm.1093, PMID:16986117.
[20] Dulai PS, Sirlin CB, Loomba R. MRI and MRE for non-invasive quantitative assessment of hepatic steatosis and fibrosis in NAFLD and NASH: Clinical trials to clinical practice. J Hepatol 2016;65(5):1006–1016. doi:10.1016/j.jhep.2016.06.005, PMID:27312947.
[21] Caussy C, Reeder SB, Sirlin CB, Loomba R. Noninvasive, Quantitative Assessment of Liver Fat by MRI-PDFF as an Endpoint in NASH Trials. Hepatology 2018;68(2):763–772. doi:10.1002/hep.29797, PMID:29356032.
[22] Haimerl M, Utpatel K, Verloh N, Zeman F, Fellner C, Nickel D, *et al*. Gd-EOB-DTPA-enhanced MR relaxometry for the detection and staging of liver fibrosis. Sci Rep 2017;7:41429. doi:10.1038/srep41429, PMID:28128291.
[23] Kukuk GM, Schaefer SG, Fimmers R, Hadizadeh DR, Ezziddin S, Spengler U, *et al*. Hepatobiliary magnetic resonance imaging in patients with liver disease: correlation of liver enhancement with biochemical liver function tests. Eur Radiol 2014;24(10):2482–2490. doi:10.1007/s00330-014-3291-x, PMID:25030459.

[24] Hoffman DH, Ayoola A, Nickel D, Han F, Chandarana H, Shanbhogue KP. T1 mapping, T2 mapping and MR elastography of the liver for detection and staging of liver fibrosis. Abdom Radiol (NY) 2020;45(3):692–700. doi:10.1007/s00261-019-02382-9, PMID:31875241.
[25] McDonald N, Eddowes PJ, Hodson J, Semple SIK, Davies NP, Kelly CJ, *et al*. Multiparametric magnetic resonance imaging for quantitation of liver disease: a two-centre cross-sectional observational study. Sci Rep 2018;8(1):9189. doi:10.1038/s41598-018-27560-5, PMID:29907829.
[26] Guimaraes AR, Siqueira L, Uppal R, Alford J, Fuchs BC, Yamada S, *et al*. T2 relaxation time is related to liver fibrosis severity. Quant Imaging Med Surg 2016;6(2):103–114. doi:10.21037/qims.2016.03.02, PMID:27190762.
[27] Unal E, Idilman IS, Karçaaltıncaba M. Multiparametric or practical quantitative liver MRI: towards millisecond, fat fraction, kilopascal and function era. Expert Rev Gastroenterol Hepatol 2017;11(2):167–182. doi:10.1080/17474124.2017.1271710, PMID:27937040.
[28] Huh J, Ham SJ, Cho YC, Park B, Kim B, Woo CW, *et al*. Gadoxetate-enhanced dynamic contrast-enhanced MRI for evaluation of liver function and liver fibrosis in preclinical trials. BMC Med Imaging 2019;19(1):89. doi:10.1186/s12880-019-0378-5, PMID:31729971.
[29] Masi B, Perles-Barbacaru TA, Laprie C, Dessein H, Bernard M, Dessein A, *et al*. Correction: In Vivo MRI Assessment of Hepatic and Splenic Disease in a Murine Model of Schistosmiasis. PLoS Negl Trop Dis 2015;9(10):e0004174. doi:10.1371/journal.pntd.0004174, PMID:26474175.
[30] Yamada T, Obata A, Kashiwagi Y, Rokugawa T, Matsushima S, Hamada T, *et al*. Gd-EOB-DTPA-enhanced-MR imaging in the inflammation stage of nonalcoholic steatohepatitis (NASH) in mice. Magn Reson Imaging 2016;34(6):724–729. doi:10.1016/j.mri.2016.03.009, PMID:26979540.
[31] Lv J, Xu Y, Xu L, Nie L. Quantitative Functional Evaluation of Liver Fibrosis in Mice with Dynamic Contrast-enhanced Photoacoustic Imaging. Radiology 2021;300(1):89–97. doi:10.1148/radiol.2021204134, PMID:33904773.
[32] Li Q, Chen K, Huang W, Ma H, Zhao X, Zhang J, *et al*. Minimally invasive photothermal ablation assisted by laparoscopy as an effective preoperative neoadjuvant treatment for orthotopic hepatocellular carcinoma. Cancer Lett 2021;496:169–178. doi:10.1016/j.canlet.2020.09.024, PMID:32987139.
[33] Yu Q, Huang S, Wu Z, Zheng J, Chen X, Nie L. Label-Free Visualization of Early Cancer Hepatic Micrometastasis and Intraoperative Image-Guided Surgery by Photoacoustic Imaging. J Nucl Med 2020;61(7):1079–1085. doi:10.2967/jnumed.119.233155, PMID:31806769.
[34] Chen DQ, Feng YL, Cao G, Zhao YY. Natural Products as a Source for Antifibrosis Therapy. Trends Pharmacol Sci 2018;39(11):937–952. doi:10.1016/j.tips.2018.09.002, PMID:30268571.
[35] Gillessen A, Schmidt HH. Silymarin as Supportive Treatment in Liver Diseases: A Narrative Review. Adv Ther 2020;37(4):1279–1301. doi:10.1007/s12325-020-01251-y, PMID:32065376.
[36] Tighe SP, Akhtar D, Iqbal U, Ahmed A. Chronic Liver Disease and Silymarin: A Biochemical and Clinical Review. J Clin Transl Hepatol 2020;8(4):454–458. doi:10.14218/jcth.2020.00012, PMID:33447529.
[37] Karimi G, Hassanzadeh-Josan S, Memar B, Esmaeili SA, Riahi-Zanjani B. Immunomodulatory effects of silymarin after subacute exposure to mice: A tiered approach immunotoxicity screening. J Pharmacopuncture 2018;21(2):90–97. doi:10.3831/KPI.2018.21.011, PMID:30151309.
[38] Demiroren K, Basunlu MT, Erten R, Cokluk E. A comparison of the effects of thymoquinone, silymarin and N-acetylcysteine in an experimental hepatotoxicity. Biomed Pharmacother 2018;106:1705–1712. doi:10.1016/j.biopha.2018.07.125, PMID:30119245.
[39] Brunt EM. Grading and staging the histopathological lesions of chronic hepatitis: the Knodell histology activity index and beyond. Hepatology 2000;31(1):241–246. doi:10.1002/hep.510310136, PMID:10613753.
[40] Delire B, Stärkel P, Leclercq I. Animal Models for Fibrotic Liver Diseases: What We Have, What We Need, and What Is under Development. J Clin Transl Hepatol 2015;3(1):53–66. doi:10.14218/JCTH.2014.00035, PMID:26357635.
[41] Bao YL, Wang L, Pan HT, Zhang TR, Chen YH, Xu SJ, *et al*. Animal and Organoid Models of Liver Fibrosis. Front Physiol 2021;12:666138. doi:10.3389/fphys.2021.666138, PMID:34122138.
[42] Nathwani R, Mullish BH, Kockerling D, Forlano R, Manousou P, Ameet D. A review of liver fibrosis and emerging therapies. European Medical Journal 2019;4(4):105–116.
[43] Luetkens JA, Klein S, Träber F, Schmeel FC, Sprinkart AM, Kuetting DLR, *et al*. Quantification of Liver Fibrosis at T1 and T2 Mapping with Extracellular Volume Fraction MRI: Preclinical Results. Radiology 2018;288(3):748–754. doi:10.1148/radiol.2018180051, PMID:29944086.
[44] Fierro-Fine A, Guerin L, Hicsasmaz H, Brown KE. Clinical Factors Associated with Hepatocellular Iron Deposition in End-stage Liver Disease. J Clin Transl Hepatol 2020;8(3):231–239. doi:10.14218/jcth.2020.00022, PMID:33083244.
[45] Gheith I, El-Mahmoudy A. Hepcidin-orchestrated Hemogram and Iron Homeostatic Patterns in Two Models of Subchronic Hepatic injury. Biomed Environ Sci 2019;32(3):153–161. doi:10.3967/bes2019.022, PMID:30987689.
[46] Mehta KJ, Farnaud SJ, Sharp PA. Iron and liver fibrosis: Mechanistic and clinical aspects. World J Gastroenterol 2019;25(5):521–538. doi:10.3748/wjg.v25.i5.521, PMID:30774269.
[47] d'Assignies G, Paisant A, Bardou-Jacquet E, Boulic A, Bannier E, Lainé F, *et al*. Non-invasive measurement of liver iron concentration using 3-Tesla magnetic resonance imaging: validation against biopsy. Eur Radiol 2018;28(5):2022–2030. doi:10.1007/s00330-017-5106-3, PMID:29178028.
[48] França M, Carvalho JG. MR imaging assessment and quantification of liver iron. Abdom Radiol (NY) 2020;45(11):3400–3412. doi:10.1007/s00261-020-02574-8, PMID:32435848.
[49] Clichici S, Olteanu D, Nagy AL, Oros A, Filip A, Mircea PA. Silymarin inhibits the progression of fibrosis in the early stages of liver injury in CCl_4-treated rats. J Med Food 2015;18(3):290–298. doi:10.1089/jmf.2013.0179, PMID:25133972.
[50] Zhao XA, Chen GM, Liu Y, Chen YX, Wu HY, Chen J, *et al*. Inhibitory effect of silymarin on CCl4-induced liver fibrosis by reducing Ly6Chi monocytes infiltration. Int J Clin Exp Pathol 2017;10(12):11941–11951. PMID:31966559.